

Soft x-ray monochromator with a varied-space plane grating for synchrotron radiation: design and evaluation

Masaaki Itou, Tatsuo Harada, and Toshiaki Kita

A soft x-ray monochromator was developed for synchrotron radiation and installed at the Photon Factory in the National Laboratory for High Energy Physics. This monochromator consists of only two optical elements: a plane mirror and a varied-space plane grating with focusing properties. The 0.7–10-nm wavelength range can be covered with resolutions of 640 at 1.4 nm and 1200 at 5 nm. The output photon flux at wavelengths above 1 nm is $\sim 10^{10}$ – 10^{11} photons/s for a 100-mA beam current in the 1% spectral bandwidth.

I. Introduction

Electrons that circulate in a storage ring emit electromagnetic radiation called synchrotron radiation (SR). Spectral continuity and high brightness of SR have enabled spectroscopic experiments to be carried out over the whole soft x-ray region. Various kinds of monochromator¹ have been constructed to obtain high photon flux from SR. Among them, plane grating monochromators^{2–5} (PGMs) have the advantages of broad spectral range and high throughput. A PGM generally consists of three optical elements: a pre-mirror, a plane grating with equally spaced grooves, and a focusing mirror. This focusing mirror with either a paraboloid or an ellipsoid surface, critically affects spectral quality. However, it is extremely difficult to fabricate such an aspheric mirror with a correct shape and a smooth surface. Thus, conventional PGMs have not yet achieved a theoretically possible resolution.

It is known that a grating whose substrate is straight, i.e., not curved, in the dispersion plane can focus a spectrum if the groove spacing varies properly with the groove position. Aspnes⁶ investigated a cylindrical grating with focusing properties provided by exponentially spaced grooves. Hettrick *et al.*^{7,8} designed an extreme ultraviolet spectrometer using a varied-space plane grating with flat field focusing. This grating was evaluated experimentally and the results were satisfactory.

We designed and built a soft x-ray monochromator^{9–11} taking advantage of the focusing properties of a varied-

space plane grating. This monochromator uses only two optical elements: a plane mirror and a plane grating ruled by a numerically controlled ruling engine.¹² Since a plane surface is easy to fabricate, a good-quality spectral image can be obtained. In addition, reduction in the number of reflections improves throughput. The monochromator is now operating at the Photon Factory in the National Laboratory for High Energy Physics. This paper presents the design details and performance of the monochromator.

II. Focusing Properties of a Varied-Space Plane Grating

In this section we describe the focusing properties of a varied-space plane grating by using the light path function.¹³ The optical system is schematically shown in Fig. 1. Let the origin O of the Cartesian coordinate system be the center of the grating, the x axis be the normal to the grating surface at O , and the y and z axes be perpendicular and parallel to the groove at O , respectively. We confine ourselves to a configuration where a source point and an image point of the principal ray lie in the x - y plane. For source point A , any point $P(o,w,l)$ on the n th groove from the groove passing through O and image point B of the principal ray, the light path function F is given by

$$F = \langle AP \rangle + \langle PB \rangle + nm\lambda, \quad (1)$$

where $\langle AP \rangle$ and $\langle PB \rangle$ are the distances from point P to points A and B , respectively; and m and λ are the spectral order and wavelength of the diffracted light. Note that the sign of n is identical to that of w . Also note that m is positive for the inside order whose diffracted beam is on the same side of the zero-order reflection as is the incident beam.

The distances $\langle AP \rangle$ and $\langle PB \rangle$ are expressed by

$$\langle AP \rangle^2 = r_1^2 + w^2 + l^2 - 2wr_1 \sin\alpha, \quad (2)$$

$$\langle PB \rangle^2 = r_2^2 + w^2 + l^2 - 2wr_2 \sin\beta, \quad (3)$$

The authors are with Hitachi, Ltd., Central Research Laboratory, Kokubunji, Tokyo 185, Japan.

Received 25 March 1988.

0003-6935/89/010146-08\$02.00/0.

© 1989 Optical Society of America.

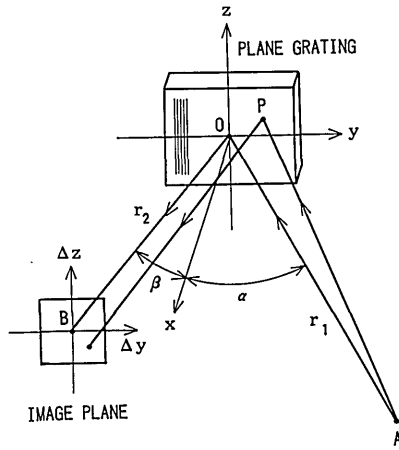


Fig. 1. Schematic diagram of the optical system.

where r_1 and r_2 are the distances from point O to points A and B , respectively; and α and β are the angles of incidence and diffraction of the principal ray. Note that α is always positive. Also note that β is either positive or negative according to whether point B is on the same side of the x axis as point A .

We determine the relation between the groove number n and the groove position w by

$$n = \frac{1}{\sigma_0} (w + b_2 w^2 + b_3 w^3 + b_4 w^4 + \dots), \quad (4)$$

where σ_0 is the groove spacing at O , and $b_i (i = 2, 3, 4, \dots)$ are the space variation parameters. These parameters can be chosen freely within the capability of the numerically controlled ruling engine. Note that the groove spacing σ is given by

$$\sigma = \frac{\sigma_0}{1 + 2b_2 w + 3b_3 w^2 + 4b_4 w^3 + \dots}. \quad (5)$$

Substituting Eqs. (2), (3), and (4) into Eq. (1), we obtain the light path function as a power series of w and l :

$$F = r_1 + r_2 + wF_{10} + w^2F_{20} + l^2F_{02} + w^3F_{30} + wl^2F_{12} + w^4F_{40} + \dots \quad (6)$$

Each $F_{ij} (i, j = 0, 1, 2, \dots)$ is expressed by

$$F_{ij} = C_{ij} + \frac{m\lambda}{\sigma_0} M_{ij}. \quad (7)$$

The explicit expressions of C_{ij} and M_{ij} are

$$C_{10} = -\sin\alpha - \sin\beta, \quad (8)$$

$$C_{20} = \frac{1}{2} \left(\frac{\cos^2\alpha}{r_1} + \frac{\cos^2\beta}{r_2} \right), \quad (9)$$

$$C_{02} = \frac{1}{2} \left(\frac{1}{r_1} + \frac{1}{r_2} \right), \quad (10)$$

$$C_{30} = \frac{1}{2} \left(\frac{\sin\alpha \cos^2\alpha}{r_1^2} + \frac{\sin\beta \cos^2\beta}{r_2^2} \right), \quad (11)$$

$$C_{12} = \frac{1}{2} \left(\frac{\sin\alpha}{r_1^2} + \frac{\sin\beta}{r_2^2} \right), \quad (12)$$

$$C_{40} = \frac{1}{8} \left(\frac{4 \sin^2\alpha \cos^2\alpha - \cos^4\alpha}{r_1^3} + \frac{4 \sin^2\beta \cos^2\beta - \cos^4\beta}{r_2^3} \right), \quad (13)$$

$$M_{10} = 1, \quad (14)$$

$$M_{20} = b_2, \quad (15)$$

$$M_{02} = 0, \quad (16)$$

$$M_{30} = b_3, \quad (17)$$

$$M_{12} = 0, \quad (18)$$

$$M_{40} = b_4. \quad (19)$$

In Eq. (6), F_{10} concerns the direction of the principal ray as follows:

$$\sin\alpha + \sin\beta = \frac{m\lambda}{\sigma_0}. \quad (20)$$

Moreover, F_{20} relates to defocus, F_{02} to astigmatism, F_{30} to coma, F_{12} to astigmatic coma, and the other F_{ij} to higher-order aberrations. The image plane is perpendicular to the principal ray and contains point B . In this plane, the image deviations Δy and Δz (parallel and perpendicular to the dispersion direction, respectively) from point B are given by

$$\Delta y = \frac{r_2}{\cos\beta} \frac{\partial F}{\partial w}, \quad (21)$$

$$\Delta z = r_2 \frac{\partial F}{\partial l}. \quad (22)$$

It can be seen that, when $F_{ij} = 0$, the related aberration vanishes. The essential point is that C_{ij} depends only on the geometric configuration, while $M_{ij} (j = 0)$ can be chosen to eliminate the aberration at one wavelength. Thus, the varied-space plane grating can focus a spectrum perfectly in the x - y plane at the specific wavelength even though neither astigmatism nor astigmatic coma can be corrected. It should be emphasized that even at other wavelengths, the same grating can satisfy the most significant focusing condition, $F_{20} = 0$, by changing either of the geometric parameters: r_1 , r_2 , α , and β .

III. Design of the Monochromator

The requirements of the experiment and the characteristics of the SR lead to the following design considerations.

(1) The monochromator is placed ~ 22 m from the source. The source size is estimated as 4.5 mm horizontally by 1.5 mm vertically. This source size is 4 orders of magnitude smaller than the distance between the source and the monochromator. Thus, as in other PGMs, the source is assumed to be an entrance slit to eliminate a mirror which would collect radiation into an entrance slit.

(2) Since the vertical source size is smaller than the horizontal one, an optical arrangement with vertical dispersion is used to obtain higher resolution. This arrangement also improves throughput because the SR is highly polarized with its electric vector in the horizontal plane and reflectivity is higher for s -polarized light than for p -polarized light.

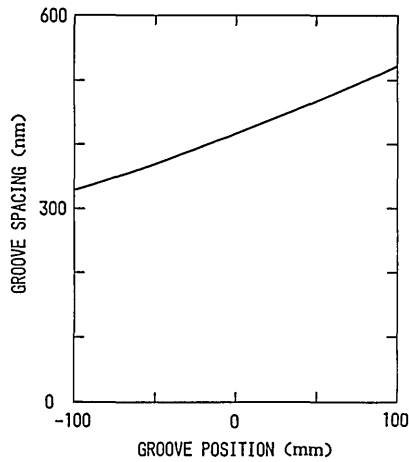


Fig. 2. Space variation of the grating.

(3) The SR is deflected horizontally by a platinum-coated plane mirror 11 m from the source to remove unwanted hard x rays. This beam deflector mirror is 360 mm long with an 89° angle of incidence. It limits the horizontal angular acceptance to 0.54 mrad. As a result, the horizontal beam-width is only 16 mm at the monochromator. Thus, focusing is not necessarily in the horizontal plane.

(4) Neither the source nor the experimental setup behind the monochromator can be moved. Thus, the directions of the incoming and outgoing beams of the monochromator and the position of the exit slit must be fixed.

(5) The monochromator must operate in ultrahigh vacuum (UHV) to prevent carbon contamination on the reflecting surfaces and to avoid deterioration of the vacuum in the storage ring. For this purpose a simple mechanism for wavelength scanning is desirable.

The design goal of the monochromator is in the 0.5–10-nm wavelength range with a resolution of ~ 1000 . High throughput is also desirable. To avoid reducing throughput, the number of optical elements must be minimized. Furthermore, an aspheric element should not be used because it is extremely difficult to fabricate.

On the basis of these considerations, we designed a monochromator with a varied-space plane grating. The space variation of the grating was determined such that the inside first-order spectrum focuses perfectly at a wavelength of 0.5 nm with the following configuration. The distances from the grating center to the source and an image point are 22.3 and 1 m, respectively. The angle of incidence is 89° , with which sufficiently high reflectivity can be expected if the groove profiles are adequate. The groove spacing at the center is 1/2400 mm. Using these values, we obtained the space variation parameters: $b_2 = -1.13185 \times 10^{-3} \text{ mm}^{-1}$, $b_3 = 1.12438 \times 10^{-6} \text{ mm}^{-2}$, and $b_4 = -1.12237 \times 10^{-9} \text{ mm}^{-3}$. Here we truncated the series in Eq. (4) after the fourth-order terms in w since the effect of higher-order aberrations is negligible. The groove spacing varies from -21% to 24% of that at the center over the ruled width of 200 mm, as shown in Fig.

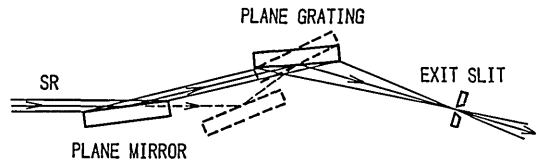


Fig. 3. Optical arrangement of the monochromator. The light source is assumed to be an entrance slit. The mirror and the grating are schematically shown for two wavelengths.

2. This space variation is readily available by using the numerically controlled ruling engine.

In a strict sense, the grating focuses a spectrum only at 0.5 nm with this configuration. However, as described in the previous section, a good-quality spectral image can be obtained by choosing an appropriate angle of incidence for each wavelength while fixing the distances from the grating center to the source and the image point. The focusing condition, $F_{20} = 0$, is expressed by

$$\frac{1}{2} \left(\frac{\cos^2 \alpha}{r_1} + \frac{\cos^2 \beta}{r_2} \right) + \frac{m\lambda b_2}{\sigma_0} = 0. \quad (23)$$

Eliminating β from Eqs. (20) and (23), we obtain the optimum angle of incidence α by

$$A \sin^2 \alpha + 2B \sin \alpha + C = 0, \quad (24)$$

$$A = \frac{1}{r_1} + \frac{1}{r_2}, \quad (25)$$

$$B = -\frac{m\lambda}{r_2 \sigma_0}, \quad (26)$$

$$C = \frac{1}{r_2} \left(\frac{m\lambda}{\sigma_0} \right)^2 - \frac{2m\lambda b_2}{\sigma_0} - \frac{1}{r_1} - \frac{1}{r_2}. \quad (27)$$

When an angle of incidence is chosen thus, the deviation angle ($\alpha - \beta$) varies for each wavelength. This implies that the source and/or the exit slit must be rotated about the grating center for wavelength scanning. To provide the fixed directions of the incoming and outgoing beams of the monochromator, we installed a plane mirror that makes a virtual source and rotates it.

The optical arrangement of the monochromator is schematically shown for two wavelengths in Fig. 3. The positions of the grating center and the exit slit are fixed. For wavelength scanning the plane mirror is translated parallel to the incoming beam and rotated about an axis in its surface to provide an appropriate deviation angle to the grating. The grating is simultaneously rotated about an axis that is parallel to the grooves and passes through its center such that an optimum angle of incidence is chosen.

The angle of incidence on the mirror θ is given by

$$\theta = \frac{1}{2}(\alpha - \beta + \delta), \quad (28)$$

where δ is the angle subtended by the incoming and outgoing beams of the monochromator. Since we have set θ to 89° at 0.5 nm, δ becomes 1.98° . As the wavelength increases from 0.5 to 10 nm, the angles of incidence on the mirror and the grating, respectively, de-

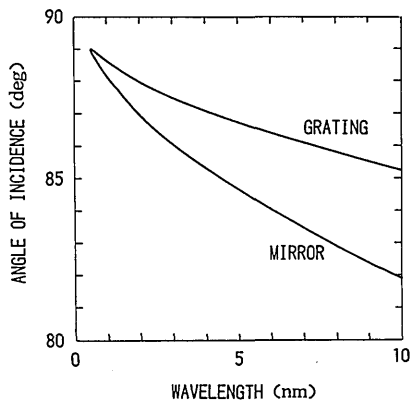


Fig. 4. Angles of incidence on the mirror and the grating.

crease from 89° to 81.9° and from 89° to 85.3° (see Fig. 4). This tendency is somewhat effective for reducing higher-order light.

The mirror and the grating are coated with gold and have the same reflecting size: 200 mm in the vertical plane by 20 mm in the horizontal plane. These elements can receive a larger vertical divergence at a longer wavelength. However, a diaphragm limits the vertical angular acceptance to 0.15 mrad to suppress the effect of residual aberrations (F_{30}, F_{40}, \dots) on the spectral image. The acceptance can be increased to obtain higher throughput at the expense of resolution. The horizontal angular acceptance is 0.54 mrad as described previously.

This monochromator has two unique properties. The first is that the magnification of the grating ($r_2/r_1)(\cos\alpha/\cos\beta)$ is nearly independent of wavelength. This property is advantageous with regard to source and slit width considerations. The second is that the zero-order light does not focus as only plane elements are used. This zero-order image expands to ~ 5 mm at the exit slit plane. However, this size is much smaller than the distance between the zero-order and first-order images (e.g., 35 mm at 0.5 nm). Thus, this property causes no extra increase in stray light.

Groove profiles of a grating strongly affect diffraction efficiency. In particular, the choice of blaze angle is important for a blazed grating with triangular groove profiles. The blaze condition, under which maximum efficiency can be obtained, occurs when the incident beam and the diffracted beam are equally inclined to the groove facets:

$$\alpha + \beta = 2\theta_B, \quad (29)$$

where θ_B is the blaze angle. Since $\alpha + \beta$ varies from 2° to 8.7° with increasing wavelength at 0.5–10 nm, the grating operates in the blaze maximum only at one wavelength. However, the variation of $\alpha + \beta$ is smaller than that for a grating used with a constant angle of incidence. Groove profiles of the grating measured by a scanning electron microscope are shown in Fig. 5.¹⁴ We found that the blaze angle is $\sim 2^\circ$; this yields a blaze wavelength of 2 nm.

The mechanical arrangement of the monochromator is schematically shown in Fig. 6. The mirror and the

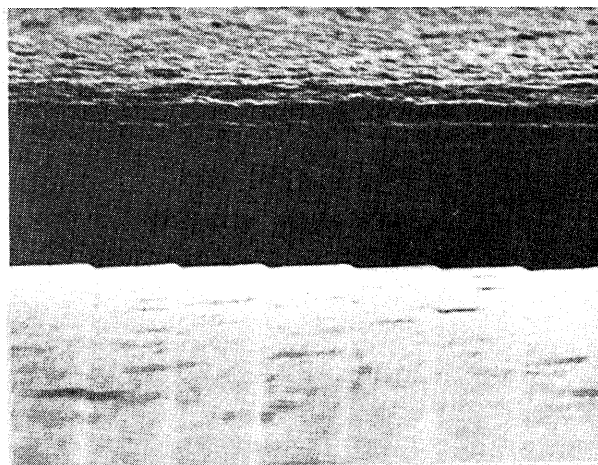


Fig. 5. Groove profiles of the grating measured by a scanning electron microscope. The groove spacing is 450 nm; the blaze angle is 2° .

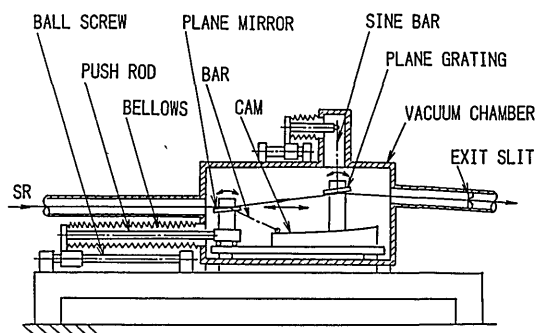


Fig. 6. Mechanical arrangement of the monochromator.

grating are installed in a vacuum chamber. A push rod translates the mirror carriage and a cam mechanism rotates the mirror with its translation. A sine bar mechanism rotates the grating. The motions are actuated from outside vacuum under computer control. To scan the entire wavelength range, the mirror is translated by 750 mm and rotated by 7.1° ; the grating is rotated by 10.5° . The mechanical construction is UHV compatible. The base pressure is $< 2 \times 10^{-7}$ Pa. An external view of the monochromator is shown in Fig. 7.

IV. Theoretical Evaluation

In the optical design we assumed a point source and considered neither the effects of residual aberrations nor the finite groove length. To estimate the resolution of the monochromator we carried out ray tracing, taking into account the finite sizes of the source and the optical elements. It is estimated that the density of emitting points of the source has a Gaussian distribution in both the horizontal and vertical directions whose standard deviation is 1.94 and 0.64 mm, respectively. For simplicity the source size is assumed to be 4.5 mm horizontally by 1.5 mm vertically. This corresponds to full width at half-maximum (FWHM) of the distribution. This rectangular source is divided into 3

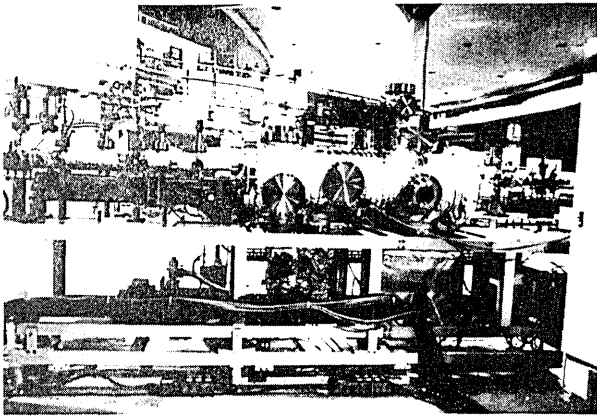


Fig. 7. External view of the monochromator.

$\times 3$ arrays, and nine points are taken at the apexes of the arrays. Each point uniformly emits 9×9 rays within 0.54 mrad (horizontal) and 0.15 mrad (vertical).

Spot diagrams, i.e., intersections of rays with an exit slit plane, are shown in Fig. 8 for wavelengths of 0.5, 1, 5, and 10 nm. Three sets of spots can be seen for each wavelength. The central set represents the images of the source points that lie in the vertical center. The upper and lower sets represent the images of the points above and below the vertical center, respectively. The width of the central images increases up to $4 \mu\text{m}$ in the dispersion direction (vertically) with wavelength due to the residual aberrations. The width of the upper and lower images is larger than that of the central ones by 1–5 μm , because the focusing condition, $F_{20} = 0$, cannot be satisfied. Nevertheless, the size of the whole images does not depend primarily on the aberrations but on the source size. It should also be emphasized that the finite groove length does not affect resolution since the images are straight horizontally. The calculated image width and the resolution $\lambda/\Delta\lambda$ are shown as a function of wavelength in Fig. 9. Here λ is the wavelength, and $\Delta\lambda$ is the product of the image width and the reciprocal linear dispersion. The predicted image size is 25–31 μm . A resolution of 840–3300 can be expected over the 0.5–10-nm wavelength range.

We estimated transmittance of the monochromator, i.e., the ratio of the output photon flux to the input photon flux, for the case where the slit width is much larger than the image width. Since every ray passes through the exit slit geometrically, transmittance T is given by

$$T = R_M R_G \epsilon, \quad (30)$$

where R_M and R_G are the reflectivities of gold at the angles of incidence on the mirror and the groove facets of the grating, respectively, and ϵ is the diffraction efficiency of the grating. The calculated reflectivities of the mirror and the grating are shown as a function of wavelength in Fig. 10. In the calculation we assumed the clean and smooth reflecting surfaces and used the atomic scattering factor published by Henke *et al.*¹⁵

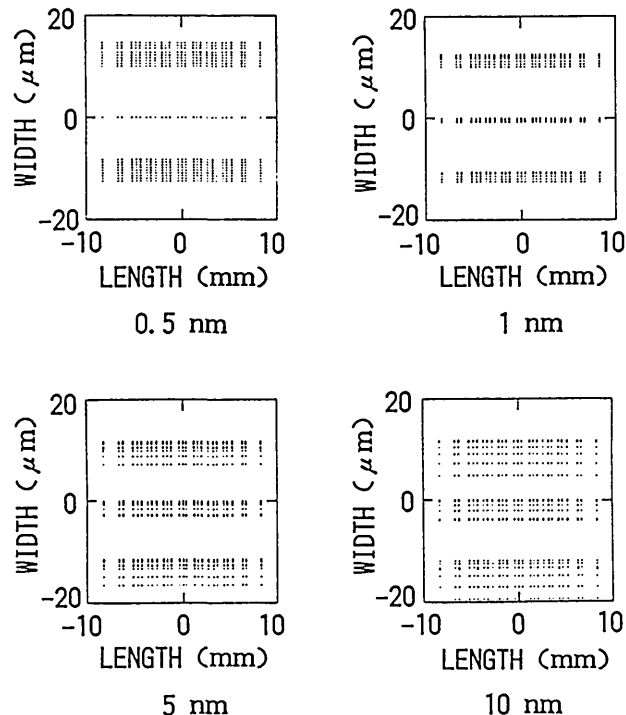


Fig. 8. Ray-traced spectral images at the exit slit plane. The source size is assumed to be 4.5 mm horizontally by 1.5 mm vertically.

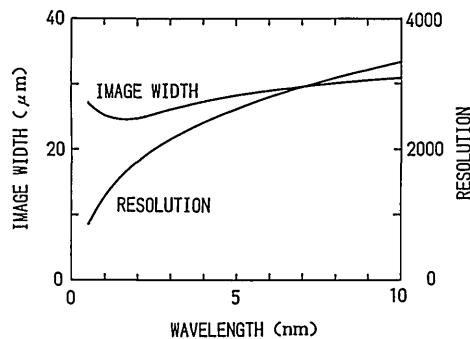


Fig. 9. Calculated image width and resolution.

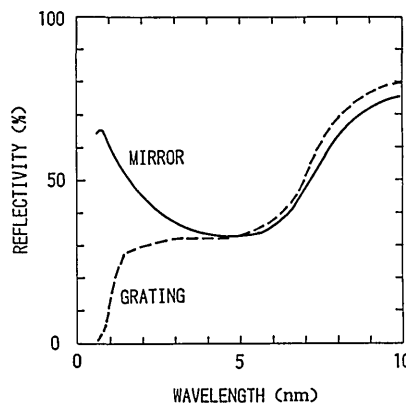


Fig. 10. Calculated reflectivities of the mirror and the grating.

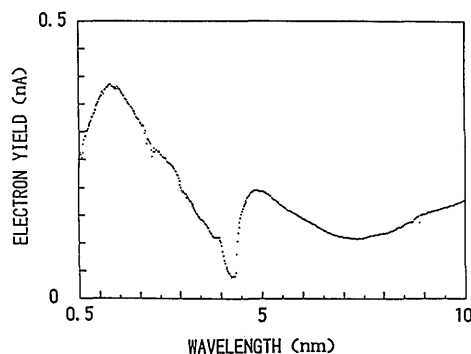


Fig. 11. Spectrum of the output intensity measured by a gold photocathode. Data include the contributions from stray light and higher-order light.

The reflectivity of the mirror varies from 33% to 76% in the 0.5–10-nm wavelength range. The reflectivity of the grating reaches its maximum of 80% at 10 nm, but it is only a few percent at wavelengths below 1 nm. This indicates that a blaze angle of 2° is too large to cover the 0.5–1-nm range. Diffraction efficiency is, in general, highly complex to calculate. However, it can be predicted with good accuracy at the blaze wavelength by an empirical formula: $\cos\alpha/\cos\beta$.¹⁶ This formula yields an efficiency of 34% for the grating whose blaze wavelength is 2 nm. Thus, we estimate that transmittance is $\sim 4\%$ at 2 nm. As the wavelength decreases from 1 nm the transmittance probably drops quickly because of the low reflectivity of the grating.

V. Experimental Evaluation

To evaluate the output photon flux of the monochromator, we measured electron yield from a gold photocathode radiated by the outgoing beam. A spectrum of the output intensity obtained for a slit width of 200 μm is shown in Fig. 11. The measured value is normalized to an electron beam current of 100 mA. (The beam current in the storage ring is typically 100–250 mA. Note that the measured yield includes contributions from stray light and higher-order light. A small dip and a large dip can be seen at 2.3-nm (oxygen *K* edge) and 4.4-nm (carbon *K* edge), respectively. This results from photoabsorption by contamination on the reflecting surfaces. The cracking of residual gases in the presence of the intense radiation generates this contamination. No noticeable fluctuation appears at 0.55-nm (gold *M*_{4,5} edge); this shows that monochromatic photons cannot be obtained here and that stray light is dominant. The stray light is most likely due to scattering in the zero-order reflection at the grating.

Table I. Output Photon Flux and Transmittance of the Monochromator; Data Include Possible Errors of 50–100%

Wavelength (nm)	Output photon flux (photons/s/100 mA/1%)	Transmittance (%)
1	5×10^{10}	0.7
2	5×10^{10}	1
5	8×10^{10}	3
10	2×10^{11}	10

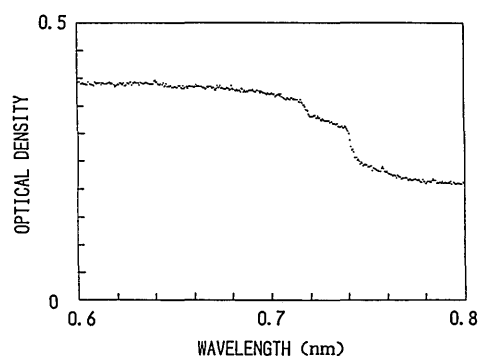


Fig. 12. Absorption spectrum of the krypton *L*_{2,3} edge. The structures at ~ 0.7 nm show that monochromatic photons are obtained.

We believe that the intensity of stray light decreases with increasing wavelength because the direction of zero-order reflection recedes from that of diffraction.

The electron yield can be converted into the photon flux by using the quantum efficiency for gold reported by Day *et al.*¹⁷ The input photon flux can also be estimated from the characteristics of the storage ring¹⁸ and the reflectivity of the beam deflector mirror. We calculated the reflectivity by using the atomic scattering factor for platinum published by Henke *et al.*¹⁵ The output photon flux normalized to a 100-mA beam current and a 1% spectral bandwidth and transmittance of the monochromator are shown in Table I. In the calculation the bandwidth was assumed to be $\Delta\lambda/\lambda$. Here $\Delta\lambda$ is the product of the slit width and the reciprocal linear dispersion, and λ is the wavelength. The results include possible errors of 50–100% because the spectral composition of the outgoing beam is not known and the quantum efficiency of the photocathode may differ from that in the literature. Nevertheless, we infer that the output photon flux is of the order of 10^{10} – 10^{11} photons/s/100 mA/1% in the 1–10-nm wavelength range. The measured transmittance is $\sim 1\%$ at 2 nm. This experimental value is considerably smaller than the 4% predicted. This is probably because the actual reflecting surfaces are neither perfectly clean nor perfectly smooth. The transmittance at 10 nm is much larger than that at 1–2 nm. This is due to the increase in reflectivities as shown in Fig. 10.

To evaluate the short-wavelength limit and resolution of the monochromator, we measured photoabsorption on several gases at the inner core levels. The *L*_{2,3} absorption spectrum of krypton is shown in Fig. 12. The structure at ~ 0.7 nm clearly show that monochromatic photons are obtained. The absorption spectra of the neon *K* edge and the argon *L*_{2,3} edge are shown in Figs. 13 and 14, respectively. These spectra are obtained for a slit width of 13 μm . The observed profile results from convolution of the instrumental function with the intrinsic absorption spectrum of the gas. The resolution of the monochromator can be derived by assuming that the instrumental function and the natural shape of the resonance line have Gaussian distributions. The natural widths of the neon $1s \rightarrow 3p$ line and the argon $2p_{3/2} \rightarrow 4s$ line are reported to be 4.9×10^{-4}

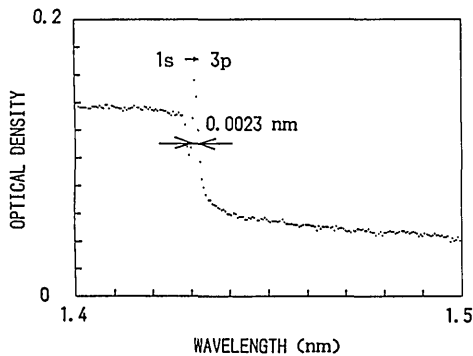


Fig. 13. Absorption spectrum of the neon K edge. The reported natural width of the $1s \rightarrow 3p$ line is 4.9×10^{-4} nm.

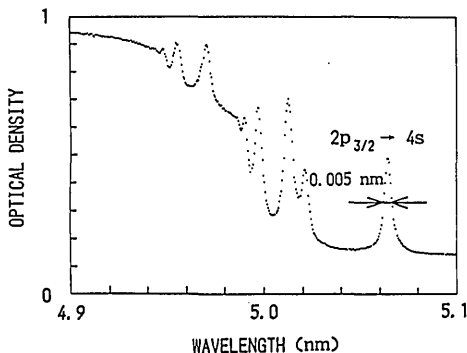


Fig. 14. Absorption spectrum of the argon $L_{2,3}$ edge. The reported natural width of the $2p_{3/2} \rightarrow 4s$ line is 2.5×10^{-3} nm.

(Ref. 19) and 2.5×10^{-3} nm,²⁰ respectively. Thus, we estimate that the resolution, i.e., the ratio of the wavelength to the FWHM of the instrumental function, is 640 at 1.4 nm and 1200 at 5 nm.

The measured resolution is half of the predicted one. The reason for this discrepancy is probably misalignment of the optics. The focusing properties of the grating strongly depend on angle of incidence. Consider the case where an angle of incidence differs from the optimum one by a small amount $\Delta\alpha$. (For simplicity, the wavelength is assumed to be unchanged.) Differentiating Eqs. (20) and (23) with respect to α and combining the results, we have

$$\frac{dr_2}{d\alpha} = \frac{2r_2 \cos\alpha(r_1 \sin\beta - r_2 \sin\alpha)}{r_1 \cos^2\beta}. \quad (31)$$

The focal length of the grating varies by $\Delta\alpha \times dr_2/d\alpha$. Consequently, image size s is approximately given by

$$s = s_0 + 2\alpha\Delta\alpha \frac{dr_2}{d\alpha}, \quad (32)$$

where s_0 is the image size for the optimum angle and α is the numerical aperture. For example, if we consider a wavelength of 5 nm, we obtain $s_0 = 28 \mu\text{m}$, $\alpha = 0.0049$, and $dr_2/d\alpha = 4.3 \times 10^3$ mm/rad. Thus, the discrepancy (factor of 2) with the predicted image size is attributed to an angle error of $\sim 7 \times 10^{-4}$ rad. We believe that the resolution can be improved by using a more precise scanning mechanism.

VI. Conclusions

The following conclusions are obtained from the studies described above.

(1) We investigated the focusing properties of a varied-space plane grating by using the light path function. In a given configuration, a varied-space plane grating perfectly focuses a spectrum in the dispersion plane at one wavelength. Even at other wavelengths this grating can image a spectrum without defocus by changing the configuration.

(2) We designed and built a monochromator that uses only two planes for reflecting surfaces. No aspheric surface is required. Wavelength scanning is accomplished by translation and rotation of a plane mirror and rotation of a varied-space plane grating. The grating focuses a good-quality spectrum by choosing an appropriate angle of incidence.

(3) The monochromator can cover the 0.7–10-nm wavelength range with resolutions of 640 at 1.4 nm and 1200 at 5 nm. The output photon flux is $\sim 10^{10}$ – 10^{11} photons/s/100 mA/1% at wavelengths above 1 nm.

The authors would like to thank H. Maezawa and A. Mikuni of the National Laboratory for High Energy Physics for their assistance with the experiment and their valuable discussions. They also acknowledge H. Taira of the Central Research Laboratory, Hitachi, Ltd., for measuring the groove profiles of the grating.

References

1. R. L. Johnson, "Grazing Incidence Monochromator for Synchrotron Radiation: a Review," *Nucl. Instrum. Methods A* **246**, 303 (1986).
2. W. Eberhardt, G. Kalkoffen, and C. Kunz, "Grazing Incidence Monochromator Flipper," *Nucl. Instrum. Methods* **152**, 81 (1978).
3. M. R. Howells, "Plane Grating Monochromators for Synchrotron Radiation," *Nucl. Instrum. Methods* **177**, 127 (1980).
4. H. Petersen, "The Plane Grating and Elliptical Mirror: a New Optical Configuration for Monochromators," *Opt. Commun.* **40**, 402 (1982).
5. W. R. Hunter, R. T. Williams, J. C. Rife, J. P. Kirkland, and M. N. Kabler, "A Grating/Crystal Monochromator for the Spectral Range 5 eV to 5 keV," *Nucl. Instrum. Methods* **195**, 141 (1982).
6. D. E. Aspnes, "High-Efficiency Concave-Grating Monochromator with Wavelength-Independent Focusing Characteristics," *J. Opt. Soc. Am.* **72**, 1056 (1982).
7. M. C. Hettrick and S. Bowyer, "Variable Line-Space Gratings: New Designs for Use in Grazing Incidence Spectrometers," *Appl. Opt.* **22**, 3921 (1983).
8. M. C. Hettrick, S. Bowyer, R. F. Malina, C. Martin, and S. Mrowka, "Extreme Ultraviolet Explorer Spectrometer," *Appl. Opt.* **24**, 1737 (1985).
9. T. Harada, M. Itou, and T. Kita, "A Grazing Incidence Monochromator with a Varied-Space Plane Grating for Synchrotron Radiation," *Proc. Soc. Photo-Opt. Instrum. Eng.* **503**, 114 (1984).
10. T. Harada, T. Kita, M. Itou, and H. Taira, "Mechanically Ruled Diffraction Gratings for Synchrotron Radiation," *Nucl. Instrum. Methods A* **246**, 272 (1986).
11. M. Itou, T. Harada, and T. Kita, "A Soft X-Ray Plane Grating Monochromator for Synchrotron Radiation," in *Abstracts, Eighth International Conference on Vacuum Ultraviolet Radiation Physics*, Lund, Sweden (Aug. 1986), Vol. 1, p. 289.

